Particle Swarm Optimisation of PID Control for a Ball-and-Beam System: Tuning Performance and Sensitivity to Ball Mass and Beam Length

Muhammad Afdhal Abdullah[1], Mohd Fairus Abdollah[2*], Mohamad Haniff Harun[3], Hairol Nizam Mohd Shah[4], Mohd Ali Arshad[5]

[1]Faculty of Electrical Technology and Engineering, Universiti Teknikal Malaysia Melaka, Hang Tuah Jaya, 76100 Durian Tunggal, Melaka, Malaysia

[2,3]School of Technical Foundation and Diploma Studies, Universiti Teknikal Malaysia Melaka, Hang Tuah Jaya, 76100 Durian Tunggal, Melaka, Malaysia

[4]Faculty of Artificial Intelligence and Cyber Security, Universiti Teknikal Malaysia Melaka, Hang Tuah Jaya, 76100 Durian Tunggal, Melaka, Malaysia

[5]Dynamics Enterprise, Kompleks Niaga Melaka Perdana, Bukit Katil, Melaka, Malaysia

***Corresponding Author**

DOI: https://doi.org/10.47772/IJRISS.2026.101000553

Received: 24 October 2026; Accepted: 29 October 2026; Published: 10 November 2026

ABSTRACT

The ball-and-beam system provides a useful benchmark for controller tuning, although performance predicted by idealised simulations may not transfer directly to physical hardware. This study compares proportional–integral–derivative (PID) control settings obtained from a Ziegler–Nichols-based calculation, manual refinement and particle swarm optimisation (PSO) for a small-angle, double-integrator ball-and-beam model. The recorded PSO solutions use integral squared error (ISE) and integral absolute error (IAE) objectives evaluated over five seconds. In the nominal reference-tracking comparison, the recorded ISE-based setting gives 1.77% overshoot and a 0.10 s settling time. Closed-loop analysis links its fast response to near cancellation of two slow pole–zero pairs, whereas a consistent homogeneous-sphere model shows that ball mass cancels from the ideal plant gain. To examine reliability and practical limitations, independent MATLAB reconstructions were conducted using 30 seeded PSO runs for each objective, persistent input disturbances, sensor noise, filtered derivative action and an assumed lagged, angle- and rate-limited servo. The reconstructed ISE search produced a mean final fitness of 0.01484988 with a standard deviation of 2.77×10^{-6}; IAE runs were less consistent and reached two distinct final-fitness groups. Under a persistent disturbance, the PSO-ISE controller retained approximately 3.47 mm of position error at 60 s, compared with negligible error for the manually tuned controller. Replacing ideal derivative-on-error action with filtered derivative-on-measurement action increased PSO-ISE settling time markedly, and actuator limits increased sensitivity to measurement noise. These results support the nominal benefit of PSO-assisted tuning while demonstrating the need to assess optimiser repeatability, disturbance rejection and actuator feasibility. All additional results are model-based, not hardware validation.

Keywords: ball-and-beam system, PID control, particle swarm optimisation, pole–zero analysis, parameter sensitivity

INTRODUCTION

The ball-and-beam system is a familiar example of an unstable mechanical plant. A ball accelerates along a

tilting beam when its angle changes, so keeping the ball near a desired position requires continuous feedback. The full system has nonlinear dynamics, while its small-angle approximation gives a double-integrator relationship between servo angle and ball position. This combination has made it a useful platform for control education and research (Keshmiri et al., 2012; Rahmat et al., 2010). More advanced ball-and-beam studies have also considered actuator constraints and configurations relevant to other underactuated systems (Ahmad, 2023).

Proportional–integral–derivative (PID) control offers a relatively simple way to regulate ball position, but selecting suitable gains remains challenging. Classical rules such as Ziegler–Nichols (Z–N) offer an initial set of parameters, although their assumptions do not necessarily hold for every plant (Åström & Hägglund, 2004). Manual adjustment may improve the response, but its outcome depends on the tuning procedure. Particle swarm optimisation (PSO) provides another approach by searching the controller-gain space against a specified performance criterion (Chaturvedi et al., 2024; Srivastava & Srivastava, 2022). Applications beyond the ball-and-beam system, including DC motor control, further illustrate the use of PSO for PID parameter selection (Rahayu et al., 2022).

This study first compares conventional and PSO-based gains on the same nominal model and explains the resulting responses through pole–zero analysis. It then revisits the physical parameter assessment to distinguish valid model predictions from numerical inconsistencies. Finally, independent follow-up simulations investigate the statistical repeatability of reconstructed PSO searches, rejection of a persistent disturbance, sensitivity to sensor noise and the consequences of actuator lag and constraints. The nominal targets remain less than 5% overshoot and a settling time below 3 s. The follow-up tests extend, rather than retrospectively reproduce, the original project simulations.

LITERATURE REVIEW

Control of the ball-and-Beam System

Several approaches to ball-and-beam control have been reported. Keshmiri et al. (2012) examined nonlinear and coupled dynamics and compared model-based and non-model-based control using an experimental system. Rahmat et al. (2010) evaluated conventional, modern and intelligent control strategies through mathematical modelling and MATLAB simulations. Further work has considered Takagi–Sugeno fuzzy-model-based adaptive control (Chang et al., 2013) and a two-degree-of-freedom fractional-order design (Mehedi et al., 2019). These studies demonstrate the range of available methods, while a single-loop PID controller remains a useful baseline for examining tuning behaviour.

PID Tuning With Metaheuristics

Metaheuristic algorithms provide a systematic way to explore PID gains without relying solely on manual adjustment. For the ball-and-beam system, Srivastava and Srivastava (2022) investigated hybrid PSO–gravitational search and PSO–grey wolf optimisation methods. Ahmad (2023) combined PSO and whale optimisation to tune several control configurations and reported improvements in error-based performance measures. Chaturvedi et al. (2024) compared teaching–learning-based optimisation with PSO in a cascade PID design and examined disturbance and parameter sensitivity. Altinoz and Yilmaz (2022) considered improved quantum-behaved PSO for a PID-like fuzzy controller. Related applications include digital DC motor PID tuning under network delays (Qi et al., 2020), conventional DC motor control (Rahayu et al., 2022), electro-hydraulic servo control (Feng et al., 2021) and hybrid differential-evolution/PSO design (Moharam et al., 2016). These findings also underline the importance of the chosen objective function and search configuration when interpreting an optimisation result.

Particle Swarm Optimisation and Performance Indices

In PSO, each particle represents a candidate solution and updates its position using its previous motion, its own best position and the best position found by the swarm (Gad, 2022; Shami et al., 2022). The inertia weight influences the balance between exploration and refinement; adaptive approaches have also been proposed

(Nickabadi et al., 2011). In controller tuning, a fitness function is commonly calculated from the tracking error. Integral squared error (ISE) places greater weight on large errors, whereas integral absolute error (IAE) weights error magnitude linearly. Importantly, an index evaluated over a finite time interval cannot measure behaviour that occurs after that interval.

Research Gap

Prior studies demonstrate the usefulness of optimisation-based PID tuning, but a single set of gains and a short fitness trace reveal little about repeatability or practical actuator demands. The present work combines the original nominal comparison with pole–zero and fitness-window interpretation, a physically consistent parameter assessment, and independently reconstructed robustness tests. Its contribution is a reproducible evaluation of the limitations of nominally fast PSO-assisted tuning, not a claim of a new PSO algorithm or experimental hardware validation.

METHODOLOGY

Overview of the Procedure

Figure 1 defines the ball-and-beam arrangement and its main geometric quantities. Figure 2 summarises the original model and controller comparisons. The analysis begins with the linearised servo-angle-to-position plant, then evaluates the Ziegler–Nichols (Z–N)-based, manually refined and two recorded PSO gain sets. Nominal reference tracking and pole–zero analysis are complemented by a direct five-second fitness check and model-consistent mass and length sensitivity calculations. Separate, explicitly identified MATLAB reconstructions then examine repeated PSO searches, disturbance rejection, measurement noise and illustrative servo limitations.

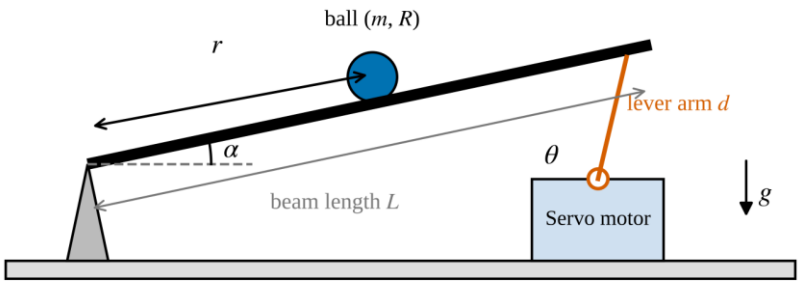


Figure 1. Schematic of the ball-and-beam system, showing servo angle θ, lever arm d, beam angle α, beam length L and ball position r.

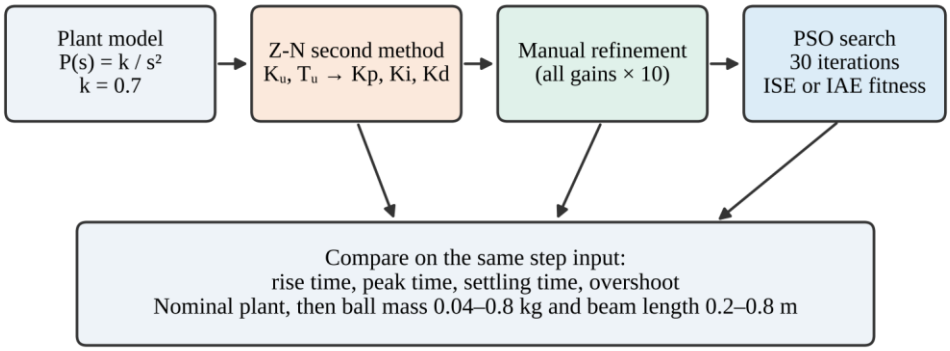


Figure 2. Study workflow, from plant modelling and controller tuning to response comparison and parameter-sensitivity assessment.

Plant Model

The model assumes ideal rolling without slipping and neglects dissipative rolling losses. Figure 1 defines the ball position r, beam angle α and other parameters used in the equation of motion. Accounting for the ball's translational and rotational inertia gives

$$\left(\frac{J}{R^2}+m\right)\ddot{r}+mg\sin\alpha-mr\dot{\alpha}^2=0 \quad (1)$$

where m is the ball mass, J its moment of inertia, R its radius and g the gravitational acceleration. For a homogeneous solid sphere, $J = 2mR^2/5$. Linearisation about a nearly horizontal beam uses $\sin\alpha \approx \alpha$ and neglects the higher-order term, giving

$$\left(\frac{J}{R^2}+m\right)\ddot{r}=mg\,\alpha \quad (2)$$

For the linkage shown in Figure 1, the small-angle relationship between servo angle θ and beam angle α is

$$\alpha=\frac{d}{L}\theta \quad (3)$$

Combining Equations (2) and (3) and taking the Laplace transform under zero initial conditions gives the transfer function from servo angle to ball position:

$$P(s)=\frac{R(s)}{\Theta(s)}=\frac{mgd}{L(J/R^2+m)}\cdot\frac{1}{s^2}=\frac{k}{s^2} \quad (4)$$

The nominal parameters are listed in Table 1. Inserting them into Equation (4) gives $k = 0.70$ m/(s²·rad), so $P(s) = 0.70/s^2$. Both open-loop poles are at the origin; a constant command therefore does not lead to a settled ball position. Importantly, if the homogeneous-ball relation $J = 2mR^2/5$ is retained when mass changes, Equation (4) simplifies to $k = 5gd/(7L)$. The resulting ideal model is independent of m for fixed geometry. This relationship is used explicitly in the parameter assessment rather than treating inertia as a fixed quantity during mass variation.

Table 1. Nominal parameters used for the ball-and-beam simulation

Parameter	Symbol	Value	Unit
Ball mass	m	0.11	kg
Ball radius	R	0.015	m
Gravitational acceleration	g	9.8	m/s²
Beam length	L	0.4	m
Lever-arm offset	d	0.04	m
Ball moment of inertia	J	9.9×10^{-6}	kg·m²

PID controller and Ziegler–Nichols tuning

The PID controller uses the error between the reference position and the measured ball position to determine the commanded servo angle. Its ideal parallel form is

$$C(s)=K_p+\frac{K_i}{s}+K_d\,s \quad (5)$$

The initial controller settings were obtained using a Ziegler–Nichols ultimate-cycle-style calculation. In this procedure, an assumed proportional gain K_u and the corresponding oscillation period T_u are inserted into the conventional tuning relationships (Ziegler & Nichols, 1942):

$$K_p = \frac{K_u}{1.7}, \quad T_i = \frac{T_u}{2}, \quad T_d = \frac{T_u}{8}, \quad K_i = \frac{K_p}{T_i}, \quad K_d = K_p T_d \tag{6}$$

For the nominal model, selecting $K_u = 10$ gives an oscillation period $T_u = 2\pi/\sqrt{(kK_u)} \approx 2.37$ s. The corresponding starting gains are $K_p = 5.88$, $K_i = 4.96$ and $K\mathcal{d} = 1.74$. Manual refinement multiplies each by ten, giving $K_p = 58.8$, $K_i = 49.6$ and $K\mathcal{d} = 17.4$. The associated closed-loop transfer function is shown in Equation (7). Because a proportional-only double integrator oscillates for every positive proportional gain, the selected K_u is not a uniquely measurable ultimate gain. The Z–N-based gain set is used here as a defined comparison baseline, not as a strict application of an ultimate-gain test. The period stated above is consistent with the model and the original oscillation plot.

$$T(s) = \frac{k(K_d s^2 + K_p s + K_i)}{s^3 + kK_d s^2 + kK_p s + kK_i} \tag{7}$$

PSO Tuning

Each PSO particle represents a candidate gain vector (K_p, K_i, $K\mathcal{d}$). Particle velocity and position are updated using the following expressions:

$$v_i^{t+1} = w\, v_i^t + c_1 r_1 (p_i - x_i^t) + c_2 r_2 (g - x_i^t) \tag{8}$$

$$x_i^{t+1} = x_i^t + v_i^{t+1} \tag{9}$$

Here, w is the inertia weight; c_1 and c_2 are the cognitive and social coefficients; r_1 and r_2 are random values between zero and one; p_i denotes the particle's own best position; and g denotes the best swarm position. The candidate gains were evaluated using either of the error-based criteria defined below:

$$\mathrm{ISE} = \int_0^T e^2(t)\, dt \tag{10}$$

$$\mathrm{IAE} = \int_0^T |e(t)|\, dt \tag{11}$$

In Equations (10) and (11), e(t) is the tracking error and T = 5 s is the original fitness window. The recorded PSO convergence trace covers 30 iterations. The accompanying project code specifies 30 particles, gain bounds of 0.01–50, $c_1 = c_2 = 2$ and inertia weight decreasing from approximately 0.9 towards 0.2. The recorded gain solutions place $K_i = 0.1$ and $K\mathcal{d} = 50$ for both objectives, with $K_p = 50$ for the recorded IAE case. As the original random seeds and complete execution record are unavailable, these curves remain historical results rather than exact replicates; the additional seeded simulations described below are independent reconstructions.

Independent PSO Repeatability Assessment

Thirty independent PSO optimisations were reconstructed for each five-second objective (ISE and IAE), using 30 particles and 30 iterations per run. The reconstructed fitness was evaluated from the nominal transfer function using the stated error definitions; individual runs were initialised with documented seeds (2001–2030 for both ISE and IAE). The gains were confined to 0.01–50 by clipping out-of-range particle positions, with

velocity limits and a decreasing inertia weight as specified in the reconstruction script. No additional swarm-diversity or restart mechanism was imposed. The final fitness distribution, mean, sample standard deviation, extrema and average global-best convergence were calculated from the 30 runs. This analysis assesses the reconstructed algorithm under known conditions; it does not claim to recover the original random optimisation trajectories.

Disturbance, Noise and Actuator Test Arrangements

The disturbance study holds the ball at a 0.20 m reference and adds a constant external acceleration of 0.10 m/s² at t = 2 s. Responses are followed to 60 s. A separate measurement-noise study applies independent Gaussian sensor noise with a standard deviation of 0.5 mm using 10 recorded seeds and a time step of 0.001 s. Both tests use the recorded gains and a filtered derivative acting on measured position (filter time constant T_f = 0.02 s), rather than an ideal derivative acting on the reference-tracking error. This avoids a reference-step derivative kick and makes the noise investigation well defined; consequently, the new responses are not directly interchangeable with the original ideal-PID results.

To examine actuation, a further simulation compares (A) the original ideal derivative-on-error controller, (B) a filtered derivative-on-measurement controller with unlimited instantaneous actuation, and (C) the same filtered controller driving an assumed first-order servo with a 0.10 s time constant, ±0.35 rad angle bounds and ±2 rad/s rate limits. The reference changes by 20 mm at t = 1 s. Tracking ISE and the integral of squared actual servo angle (ISCE = $\int\theta^2(t)dt$, over five seconds) are evaluated, together with saturation and rate-limit percentages. These illustrative servo values were not measured from a physical ball-and-beam rig and were not included as penalties in a new PSO optimisation.

Performance Measures and Test Cases

Nominal reference-tracking performance is reported using 10–90% rise time T_r, peak time T_p, 2% settling time T_s and percentage overshoot, with design targets $T_s < 3$ s and overshoot < 5%. The reference plant has m = 0.11 kg and L = 0.4 m. For the analytical mass study, $J = 2mR^2/5$ is updated consistently at each value; beam lengths of 0.2, 0.4 and 0.8 m are evaluated with fixed nominal PID gains. Table 5 gives analytical mass-invariance predictions, and Table 6 provides independent continuous-time length-response calculations. The additional validation experiments below use the same nominal plant but explicitly stated disturbance, noise and actuator assumptions.

RESULTS AND DISCUSSION

Behaviour With and Without Feedback

For the open-loop plant, a constant servo-angle input produces a position that grows with time, as expected of a double integrator. Unity position feedback without damping yields $k/(s^2 + k)$, whose poles are $\pm j\sqrt{k}$; the resulting oscillation does not settle. This explains why a suitable damping contribution is essential before the nominal tracking targets can be met.

Ziegler–Nichols and Manual Tuning

Table 2 presents the four nominal PID gain sets and the error indices calculated on the specified five-second, 0.01 s sampling grid. Their transient responses are compared in Table 3 and Figure 4; the corresponding closed-loop poles appear in Figure 5. With the Z–N-based gains, the nominal model produces about 70.7% overshoot and a 24.1 s settling time. Its lightly damped complex poles (approximately $-0.156 \pm j1.95$ s^{-1}) account for this long settling tail. Since the ideal double integrator has no uniquely defined ultimate gain under proportional-only control, this conventional gain set is best treated as an initial benchmark.

Scaling the three initial gains by ten improves the nominal response. Table 3 and Figure 4 show that overshoot falls to about 17% and settling time to 0.877 s. The poles in Figure 5 move to the negative real axis, but the overshoot remains above the 5% target. The gain-scaling exercise is therefore useful as a comparison, not

evidence that trial-and-error tuning has reached a best solution.

Table 2. Nominal controller gains and recomputed error indices over the 0–5 s evaluation interval

Controller	K_p	K_i	K_d	ISE	IAE
Z-N	5.88	4.96	1.74	1.0593	2.0491
Manual (×10)	58.8	49.6	17.4	0.0442	0.1467
PSO, ISE fitness	35.18	0.1	50	0.01487	0.0533
PSO, IAE fitness	50	0.1	50	0.01487	0.0530

ISE and IAE for all gain sets were evaluated using the nominal model, a unit-step reference and a 0.01 s trapezoidal grid over 0–5 s. The retained ISE fitness is reproduced to the reported precision. These checks establish consistency for the nominal case only.

PSO Convergence and Tuned Response

Figure 3 compares the recorded global-best fitness values for ISE and IAE across 30 PSO iterations. The ISE value falls from 0.015232 to 0.014865 by iteration 4, while the IAE value reaches 0.053081 by iteration 5. Both curves remain flat for the rest of the run. These plots show early stagnation of the recorded searches; they do not establish that either result is a global optimum.

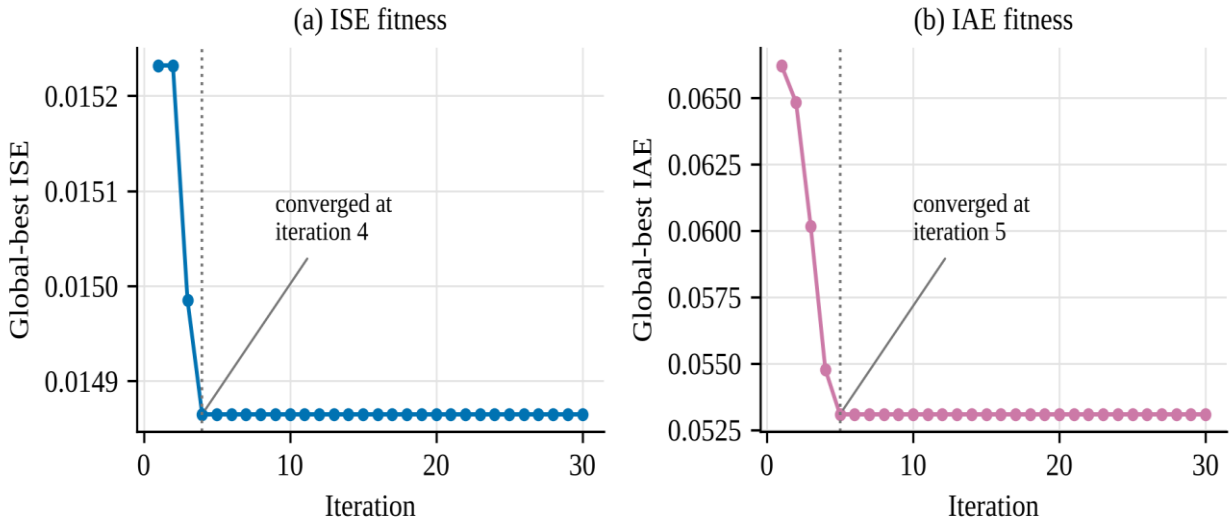


Figure 3. Recorded PSO convergence curves for (a) ISE and (b) IAE fitness.

The retained PSO gain sets meet the nominal transient targets (Table 3). The ISE-based setting gives approximately 1.77% overshoot and a 0.10 s settling time, whereas the IAE-based setting gives 2.44% and 0.434 s. Figure 4 shows their initial responses alongside the two conventional cases. These are responses of the idealised model; they should not be read as predictions of achievable servo performance without actuator or sensor dynamics.

Table 3. Transient response of the four controller settings for the nominal model

Controller	T_r (s)	T_p (s)	T_s (s)	Overshoot (%)
Z-N	0.47	1.32	24.1	70.7
Manual (×10)	0.115	0.33	0.877	17.0
PSO, ISE fitness	0.06	0.23	0.10	1.77
PSO, IAE fitness	0.058	0.21	0.434	2.44

The comparison uses a 2% settling-time criterion; values are based on the recorded gain sets and a reconstruction of the nominal-model responses.

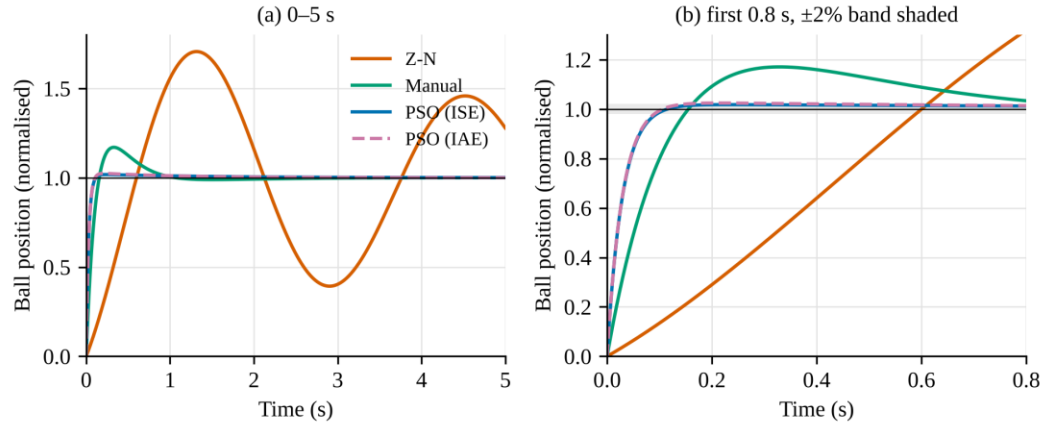


Figure 4. Nominal-model unit-step responses for the four controller settings: (a) full 5 s interval and (b) enlarged initial response.

Dynamic interpretation of the PSO settings

The ISE-based gains in Table 2 place the derivative gain close to the upper search bound and the integral gain near the lower part of the recorded solution space. For this gain set, the poles plotted in Figure 5 lie near −34.3, −0.715 and −0.003 s^{-1}; the controller zeros are close to −0.70 and −0.003 s^{-1}. The slow modes are consequently almost cancelled in the reference-to-position transfer function, leaving an approximately first-order fast response. This accounts for its short nominal settling time. The cancellation is approximate, and it should not be assumed to provide the same behaviour under unmodelled disturbances or parameter uncertainty.

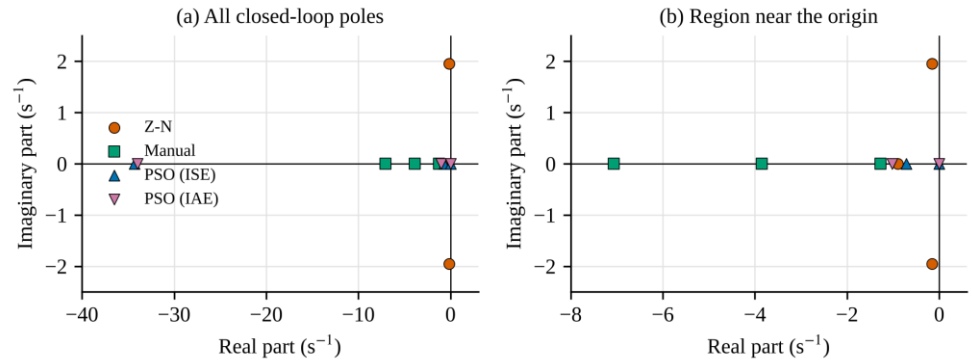


Figure 5. Closed-loop poles of the four nominal controller designs, shown (a) over the full range and (b) near the origin.

The selected derivative gain also lies at the upper limit of the accompanying PSO code, suggesting that the ideal-model fitness rewards rapid motion without an explicit control-effort cost. Hardware constraints would temper this preference: actuator bandwidth and saturation, measurement noise and derivative filtering were excluded. The small integral gain also makes the response to sustained disturbances potentially slow. The present tests assess reference tracking only.

Examination of the Optimisation Result

Figure 6 shows an independent calculation of the five-second cost as K_p varies from 1 to 50 while $K_i = 0.1$ and $K\mathcal{d} = 50$ are fixed. Over this interval the ISE is relatively flat, with a shallow minimum close to $K_p = 4.7$. The IAE decreases as K_p is reduced, so $K_p = 50$ is not the best value along this one-dimensional slice. Table 4 compares the two recorded gain sets with two illustrative candidate sets evaluated using the same model and sampling convention. These candidate values are a direct numerical cross-check; they are not presented as reproduced outcomes of a stochastic PSO run. The distinction matters because the original random seeds and a complete execution record are unavailable.

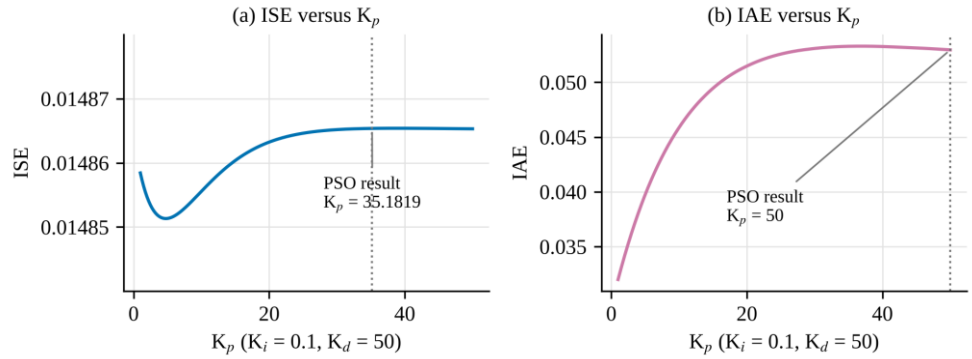


Figure 6. Five-second (a) ISE and (b) IAE as K_p varies with K_i = 0.1 and K_d = 50. Markers indicate the originally recorded PSO gain values.

A smaller fitness within a five-second window is not necessarily a better long-term response. The illustrative low-K_p IAE candidate has a weakly damped, slow oscillatory mode whose peak occurs well beyond the five-second evaluation window. Taken together, Figures 3 and 6 and Table 4 indicate that the optimisation outcome should be assessed with a sufficiently long evaluation interval and, where appropriate, penalties for slow modes or excessive control effort. The evidence does not establish a global optimum.

Table 4. Direct cost comparison for recorded and illustrative candidate gain sets

Gain set	K_p	K_i	K_d	ISE	IAE
Recorded PSO–ISE	35.18	0.1	50	0.01487	0.0533
Recorded PSO–IAE	50	0.1	50	0.01487	0.053
Illustrative ISE candidate	4.76	0.1	50	0.01485	0.0394
Illustrative IAE candidate	0.1	0.1	50	0.01486	0.0298

Recorded rows use the retained nominal gains. Candidate rows are direct evaluations of specified gains, not re-created PSO runs. The error indices use a unit-step reference, a five-second window and a 0.01 s trapezoidal grid.

Effect of ball mass and beam length

The mass and length assessments must follow the assumptions of Equation (4). For the stated homogeneous solid ball, $J = 2mR^2/5$, so m cancels and $k = 5gd/(7L)$. Table 5 gives the resulting mass and inertia pairs: although J increases with m, the plant gain remains 0.70 at the nominal beam length. The same fixed PID gains therefore give exactly the same ideal-model transfer function and step response for every listed mass. Figure 7(a) and Figure 7(c) illustrate the resulting constant settling-time and overshoot predictions. The mass-dependent changes described in the earlier numerical record arise from a different parameter-setting convention—holding J at its nominal value while changing m—and are not a physical mass-sensitivity result for a homogeneous sphere of fixed radius.

Table 5. Analytical effect of ball mass when $J = 2mR^2/5$ and L = 0.4 m

Ball mass m (kg)	Inertia J (kg·m²)	Plant gain k	PSO–ISE T_s (s)	PSO–ISE OS (%)
0.04	3.60e-06	0.70	0.10	1.77
0.11	9.90e-06	0.70	0.10	1.77
0.4	3.60e-05	0.70	0.10	1.77
0.6	5.40e-05	0.70	0.10	1.77
0.8	7.20e-05	0.70	0.10	1.77

The response values are analytical predictions of the same nominal ideal-model transfer function for every mass, not separate simulation measurements. With fixed gains, the Z–N and manual responses are likewise unchanged from Table 3.

Beam length changes the plant gain because k = 5gd/(7L). Table 6 gives model-consistent step-response calculations for L = 0.2, 0.4 and 0.8 m at fixed ball properties and unchanged nominal gains. For the ISE-based PSO case, a longer beam increases the settling time and overshoot, although all three listed lengths still meet the nominal design targets in this idealised calculation. The manually refined controller exceeds the overshoot limit throughout. More importantly, the Z–N-based loop becomes unstable for L = 0.8 m: the characteristic equation has a right-half-plane conjugate pole pair, so no finite settling time can be assigned. Figures 7(b) and 7(d) display the recalculated length trends; the unstable Z–N point is labelled rather than plotted as a valid settling time. These results replace the internally inconsistent variation values in the earlier draft.

Table 6. Recalculated length sensitivity with the nominal PID gains held fixed

Beam length L (m)	**Gain k**	**Z–N T_s / OS**	**Manual T_s / OS**	**PSO–ISE T_s / OS**
0.2	1.40	5.088 s / 48.94%	0.704 s / 9.99%	0.051 s / 0.93%
0.4	0.70	24.09 s / 70.72%	0.877 s / 17.08%	0.095 s / 1.78%
0.8	0.35	Unstable	2.035 s / 27.81%	1.133 s / 3.29%

Entries show 2% settling time and percentage overshoot from the ideal continuous-time model of Equation (7), sampled at 0.001 s. “Unstable” denotes right-half-plane poles and hence no finite settling time. The nominal row is shown at the precision of the reconstruction; Table 3 preserves the rounded recorded nominal values.

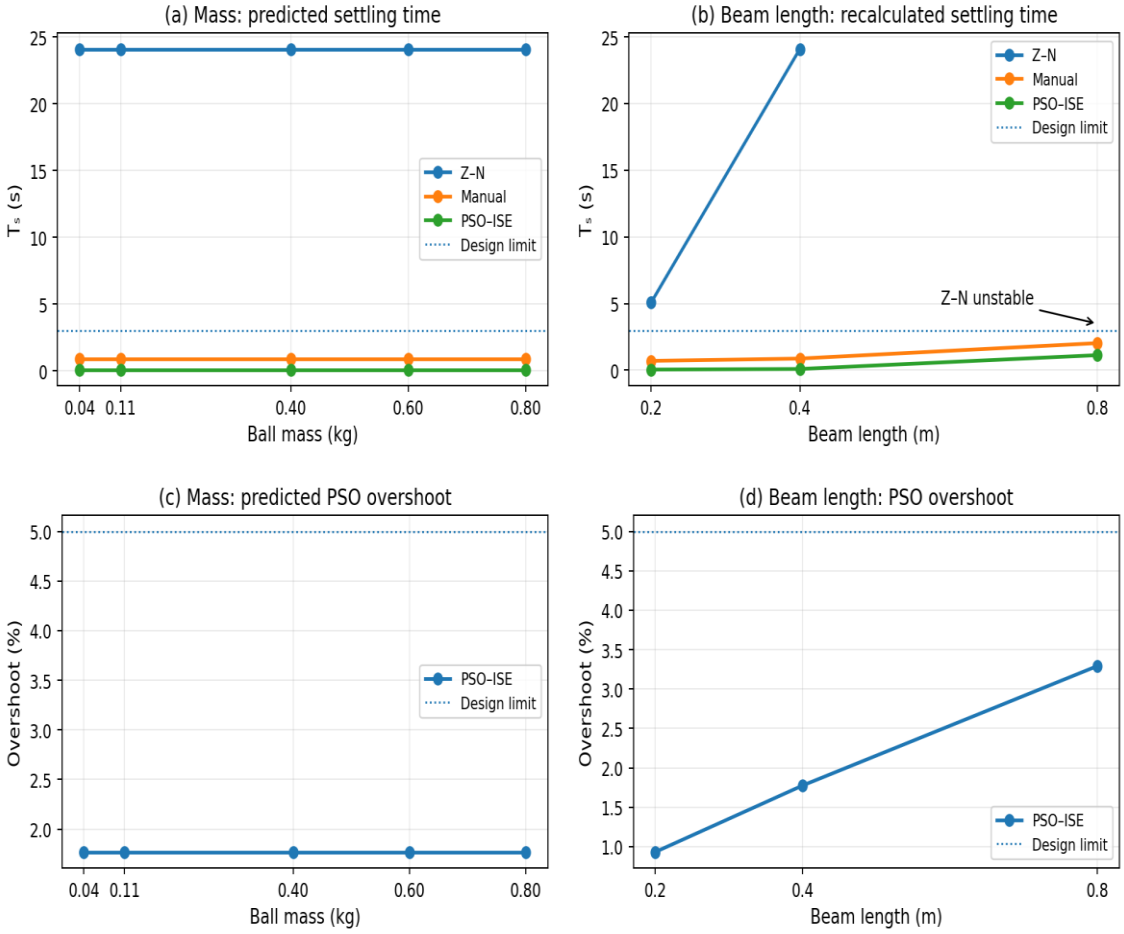


Figure 7. Model-consistent sensitivity with fixed controller gains: (a) mass-independent settling time predicted by J = 2mR²/5, (b) recalculated settling time versus beam length, (c) mass-independent PSO–ISE overshoot

and (d) PSO–ISE overshoot versus beam length. The unstable Z–N point at L = 0.8 m is identified explicitly. Dotted guides indicate the design limits.

Statistical repeatability of the reconstructed PSO

Table 7 and Figure 8 summarise 30 independent optimisation runs for each objective. The ISE search produces a tightly clustered final fitness (mean 0.01484988; sample standard deviation 2.77×10^{-6}). Twenty-nine runs terminate close to 0.01484938, while one has a higher final value near 0.01486457. The IAE search shows much greater variation (mean 0.04013267; standard deviation 0.01215221), with 16 runs reaching about 0.02895638 and 14 stopping near 0.05290557. The mean convergence traces and standard-deviation bands in Figure 8 show that different random initialisations influence the IAE outcome more strongly in this reconstruction.

Table 7. Statistical summary of 30 independent reconstructed PSO runs for each fitness objective.

Objective	Runs	Mean fitness	Std. deviation	Best fitness	Worst fitness
ISE	30	0.01484988	2.7736097e-06	0.01484938	0.01486457
IAE	30	0.04013267	0.012152206	0.02895638	0.05290557

The fitness values compare optimisation quality only within the respective ISE or IAE objective; their numerical scales should not be compared directly. Seeded runs use gain bounds 0.01–50, and not the reported historical PSO gains as initial conditions.

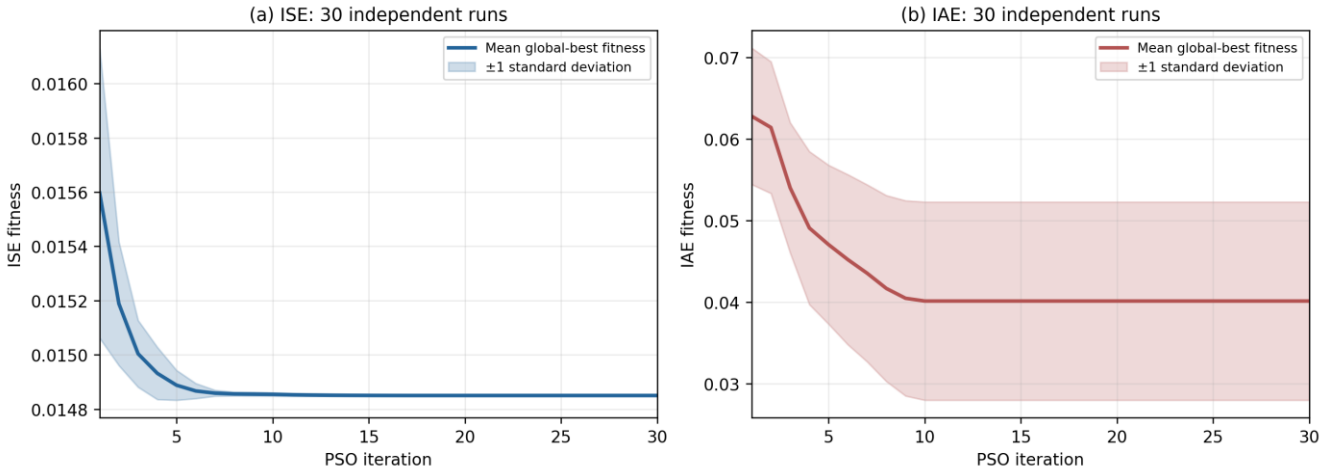


Figure 8. Independent PSO repeatability: mean global-best fitness over 30 iterations with ±1 sample standard deviation for (a) ISE and (b) IAE (30 recorded seeds per objective).

Across these reconstructions, K_i converges to 0.01 and $K\mathcal{d}$ to 50, both at the imposed gain bounds; the lower limit differs from the $K_i = 0.1$ values in the recorded historical gain sets. Similar final ISE values therefore do not imply identical gains or equivalent long-term performance. In the IAE runs, the lower-fitness solutions are associated with small proportional gains, for which slow dynamics beyond the five-second fitness window remain an important concern. The observed bimodal IAE outcomes and boundary solutions do not establish a global optimum and motivate reporting seed variation and search constraints.

Additional Disturbance, Noise and Actuator Validation

A persistent disturbance exposes limitations that are not visible in nominal step tracking. For an added acceleration of 0.10 m/s² applied at t = 2 s, the initial peak position errors are 26.51 mm (Z–N), 1.95 mm (manual), 3.99 mm (recorded PSO–ISE) and 2.83 mm (recorded PSO–IAE). The manual controller returns to and remains within ±1 mm of the target 1.46 s after the disturbance, compared with 19.07 s for the Z–N case. In contrast, at t = 60 s the PSO–ISE and PSO–IAE loops still have errors of approximately 3.47 and 2.55 mm, respectively, as illustrated in Figure 9(a). The finite-time residuals must not be described as permanent steady-

state errors; rather, they indicate very slow disturbance rejection with $K_i = 0.1$.

The 0.5 mm-standard-deviation sensor-noise test further distinguishes ball-position regulation from servo demand. Over 10 seeds, the recorded PSO–ISE controller has an average RMS actual-position fluctuation of 0.0693 mm, but its unlimited requested servo command has an RMS magnitude of 1.294 rad. The corresponding manual-controller values are 0.0481 mm and 0.471 rad. Thus, small position fluctuations can accompany considerable servo activity in the idealised unlimited-actuation model.

In the 20 mm reference-step comparison, the recorded PSO–ISE gains settle in 0.095 s with the original ideal derivative-on-error implementation (Case A). The same gains settle in 5.302 s when derivative action is filtered and applied to measured position with an unlimited actuator (Case B), and in 5.344 s with the assumed lagged and limited servo (Case C). Figure 9(b) shows that the main difference arises between Cases A and B; it would be inaccurate to attribute the entire delay to saturation. Under Case C, the PSO–ISE angle command is saturated for 9.66% of the tracking test and its servo rate is limited for 15.24%; the five-second ISCE of actual servo angle rises from 0.01217 rad²s in Case B to 0.02371 rad²s in Case C. All of these values are specific to the simulated 20 mm reference change.

Figures 9(c)–(d) summarise the more severe noise-test trade-off. Across 10 seeds, imposing the illustrative servo constraints raises PSO–ISE RMS position error from 0.0693 to 1.4597 mm while reducing RMS actual servo angle from 1.2937 to 0.0810 rad. The raw PSO–ISE commands reach the angle limit on average 79.6% of the noise-test interval and the rate limit 84.6% of the interval. In the unsaturated linear servo-lag model, the Z–N gain set has a right-half-plane pole (maximum real part about +0.0142 s^{-1}), whereas the other three gain sets remain linearly stable. The pole result is not a proof of global nonlinear behaviour under saturation. These findings evaluate control effort and feasibility after tuning; a weighted control-effort term was not incorporated into a new PSO objective.

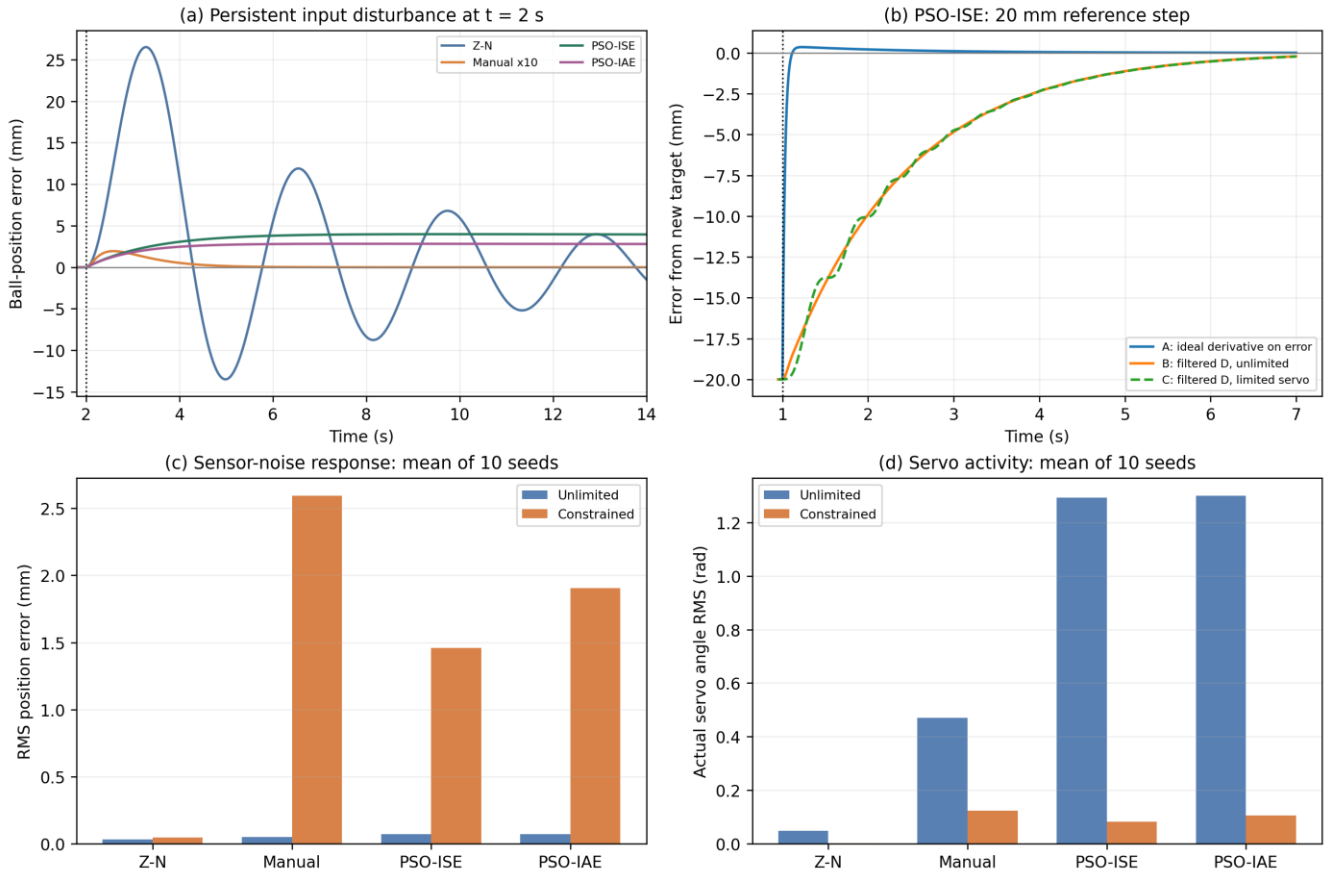


Figure 9. Independently reconstructed robustness tests: (a) persistent acceleration disturbance; (b) PSO–ISE response to a 20 mm step with ideal, filtered and constrained actuation; (c) RMS ball-position error under Gaussian sensor noise; and (d) RMS actual servo angle (10 seeded noise trials). All servo constraints are illustrative assumptions.

LIMITATIONS

This analysis is restricted to a small-angle, idealised double-integrator ball-and-beam plant and independently reconstructed simulations. The original PSO random seeds and complete execution record were unavailable; the new repeatability runs use documented seeds and the lower gain bound 0.01, whereas the recorded gain sets have $K_i = 0.1$. The statistical results therefore characterise the reconstruction, not the original optimisation. The added disturbance and noise tests employ a derivative filter and derivative-on-measurement implementation, and the actuator study assumes rather than measures servo lag, angle limits and rate limits. Consequently, it does not establish achievable performance on an actual apparatus. Control effort is measured after tuning, not used in a weighted constrained-PSO objective; sensor bandwidth, backlash, friction, ball slip and hardware saturation characteristics were not experimentally identified. The analysis focuses on input-acceleration disturbance and Gaussian measurement noise, not all possible operating conditions. Further hardware-informed tuning and experimental validation would be needed before practical performance claims could be made.

CONCLUSION AND RECOMMENDATIONS

This work compared Z–N-based, manually refined and recorded PSO-selected PID gains on a linearised ball-and-beam model. For nominal ideal reference tracking, the ISE-based PSO setting meets the overshoot and settling-time targets, aided by near cancellation of two slow pole–zero pairs. The homogeneous-sphere model predicts mass-independent dynamics for fixed geometry, while longer beams change plant gain and can destabilise the conventional gain set. The additional seeded PSO reconstruction confirms highly repeatable five-second ISE fitness but substantial run-to-run variability for IAE. Disturbance and noise tests show that fast nominal reference tracking does not guarantee rapid rejection of persistent disturbances or low servo demand. Finally, using filtered derivative action and illustrative actuator constraints markedly changes the response obtained with the original PSO gains. These comparisons support PSO as a useful nominal tuning approach while demonstrating the need for realistic control implementation, documented search settings and robustness evaluation before drawing hardware conclusions.

Future work should evaluate a longer optimisation horizon and explicitly include weighted control-effort or actuator-constraint penalties when searching for gains. Hardware-specific servo dynamics, sensor properties and derivative filtering should be identified experimentally, followed by controller retuning and validation for both reference changes and disturbance rejection. The present additional simulations offer a transparent model-based starting point but do not constitute experimental verification.

ACKNOWLEDGEMENT

The authors thank the School of Technical Foundation and Diploma Studies, Universiti Teknikal Malaysia Melaka (UTeM), for institutional and academic support during this study.

REFERENCES

1. Ahmad, N. S. (2023). Modeling and hybrid PSO-WOA-based intelligent PID and state-feedback control for ball and beam systems. IEEE Access, 11, 137866–137880. https://doi.org/10.1109/ACCESS.2023.3339879
2. Altinoz, O. T., & Yilmaz, A. E. (2022). Investigation of the optimal PID-like fuzzy logic controller for ball and beam system with improved quantum particle swarm optimization. International Journal of Computational Intelligence and Applications, 21(4), 2250025. https://doi.org/10.1142/S1469026822500250
3. Åström, K. J., & Hägglund, T. (2004). Revisiting the Ziegler–Nichols step response method for PID control. Journal of Process Control, 14(6), 635–650. https://doi.org/10.1016/j.jprocont.2004.01.002
4. Chang, Y.-H., Chan, W.-S., & Chang, C.-W. (2013). T–S fuzzy model-based adaptive dynamic surface control for ball and beam system. IEEE Transactions on Industrial Electronics, 60(6), 2251–2263. https://doi.org/10.1109/TIE.2012.2192891

5. Chaturvedi, S., Kumar, N., & Kumar, R. (2024). Two feedback PID controllers tuned with teaching–learning-based optimization algorithm for ball and beam system. IETE Journal of Research, 70(7), 6340–6349. https://doi.org/10.1080/03772063.2023.2284955
6. Feng, H., Ma, W., Yin, C., & Cao, D. (2021). Trajectory control of electro-hydraulic position servo system using improved PSO-PID controller. Automation in Construction, 127, 103722. https://doi.org/10.1016/j.autcon.2021.103722
7. Gad, A. G. (2022). Particle swarm optimization algorithm and its applications: A systematic review. Archives of Computational Methods in Engineering, 29, 2531–2561. https://doi.org/10.1007/s11831-021-09694-4
8. Keshmiri, M., Jahromi, A. F., Mohebbi, A., Amoozgar, M. H., & Xie, W.-F. (2012). Modeling and control of ball and beam system using model based and non-model based control approaches. International Journal on Smart Sensing and Intelligent Systems, 5(1), 14–35. https://doi.org/10.21307/ijssis-2017-468
9. Mehedi, I. M., Al-Saggaf, U. M., Mansouri, R., & Bettayeb, M. (2019). Two degrees of freedom fractional controller design: Application to the ball and beam system. Measurement, 135, 13–22. https://doi.org/10.1016/j.measurement.2018.11.021
10. Moharam, A., El-Hosseini, M. A., & Ali, H. A. (2016). Design of optimal PID controller using hybrid differential evolution and particle swarm optimization with an aging leader and challengers. Applied Soft Computing, 38, 727–737. https://doi.org/10.1016/j.asoc.2015.10.041
11. Nickabadi, A., Ebadzadeh, M. M., & Safabakhsh, R. (2011). A novel particle swarm optimization algorithm with adaptive inertia weight. Applied Soft Computing, 11(4), 3658–3670. https://doi.org/10.1016/j.asoc.2011.01.037
12. Qi, Z., Shi, Q., & Zhang, H. (2020). Tuning of digital PID controllers using particle swarm optimization algorithm for a CAN-based DC motor subject to stochastic delays. IEEE Transactions on Industrial Electronics, 67(7), 5637–5646. https://doi.org/10.1109/TIE.2019.2934030
13. Rahayu, E. S., Ma'arif, A., & Çakan, A. (2022). Particle swarm optimization (PSO) tuning of PID control on DC motor. International Journal of Robotics and Control Systems, 2(2), 435–447. https://doi.org/10.31763/ijrcs.v2i2.476
14. Rahmat, M. F., Wahid, H., & Wahab, N. A. (2010). Application of intelligent controller in a ball and beam control system. International Journal on Smart Sensing and Intelligent Systems, 3(1), 45–60. https://doi.org/10.21307/ijssis-2017-378
15. Shami, T. M., El-Saleh, A. A., Alswaitti, M., Al-Tashi, Q., Summakieh, M. A., & Mirjalili, S. (2022). Particle swarm optimization: A comprehensive survey. IEEE Access, 10, 10031–10061. https://doi.org/10.1109/ACCESS.2022.3142859
16. Srivastava, V., & Srivastava, S. (2022). Hybrid optimization based PID control of ball and beam system. Journal of Intelligent & Fuzzy Systems, 42(2), 919–928. https://doi.org/10.3233/JIFS-189760
17. Ziegler, J. G., & Nichols, N. B. (1942). Optimum settings for automatic controllers. Transactions of the ASME, 64(8), 759–765. https://doi.org/10.1115/1.4019264